Nonsymmetric Flight Influence on High-Angle-of-Attack Handling and Departure

Donald E. Johnston* and Jeffrey R. Hogget
Systems Technology, Inc., Hawthorne, Calif.

In high α maneuvering of high-performance military aircraft it is common for sideslip to exist either intentionally or unintentionally. Analysis and simulation of an aircraft in unsymmetric flight has resulted in identification of new open-and closed-loop parameters which relate to a coupled longitudinal-lateral divergence known as nose slice departure. The coupling produces nonminimum phase zeros in the pitch attitude numerator at angle of attack below that for stall and at relatively small sideslip angles. Pilot control of pitch attitude via elevator then produces a lateral divergence. The phenomenon is traced through the equation of motion, effective stability derivative, transfer function, and root aerodynamic flow relationships. The results are verified by open- and closed-loop time histories from a nonlinear six-degree-of-freedom digital simulation and by fixed-base piloted simulation.

Nomenclature

a_y = lateral acceleration at c.g., fps^2
$C_\ell(\alpha,\beta)$ = nondimensional rolling moment coefficient as a function of α and β; body axis system
C_{ℓ_i} = $\partial C_\ell(\alpha,\beta)/\partial_i$
$C_n(\alpha,\beta)$ = nondimensional yawing moment coefficient as a function of α and β; body axis system
C_{n_i} = $\partial C_n(\alpha,\beta)/\partial_i$
$C_{n_{\beta_{\text{dyn}}}}$ = $C_{n_\beta} - (I_z/I_x)\alpha C_{\ell_\beta}$
DOF = degrees of freedom
g = gravitational acceleration constant
h = altitude, ft
i = state variable, e.g., α, β, θ
I_x, I_z = body axis moments of inertia, slug-ft^2
K_θ = pitch attitude feedback gain
L, M, N = aerodynamic moments about conventional aircraft body axes
L_i' = total incremental change in rolling moment due to incremental change in state variable quantity
M_i = $\partial M/\partial i$
n_z = normal load factor, g
N_i' = total incremental change in yaw moment due to incremental change in state variable quantity
$N^\theta_{\delta_e}$ = numerator of pitch attitude-to-elevator transfer function, deg/deg
p,q,r = perturbed angular velocities about conventional aircraft body axes, deg/sec
s = laplace operator; $\sigma \pm j\omega$
T_R = roll subsidence time constant, sec
T_S = spiral time constant
T_{θ_1} = time constant of conventional low-frequency first-order root of $N^\theta_{\delta_e}$ (uncoupled)
T_{θ_2} = time constant of conventional high-frequency first-order root of $N^\theta_{\delta_e}$ (coupled or uncoupled)
T_{θ_3} = time constant of first-order nonminimum phase root of $N^\theta_{\delta_e}$ (coupled)
u = perturbed total linear velocity, fps
X,Y,Z = aerodynamic forces along an axis system with x axis aligned with the total velocity vector, z axis in aircraft plane of symmetry pointing down, and y axis orthogonal to x and z axes and positive out right wing
X_i, Y_i, Z_i = $\partial(\ )/\partial i$
α = perturbed angle of attack, deg
β = sideslip angle, deg
$\delta(\ )$ = surface deflection, deg
Δ = transfer function denominator
$\zeta(\ )$ = damping ratio
θ,φ,ψ = Euler angles between gravity-oriented inertial axis and aircraft body axis, deg
$\omega_{(\ )}$ = natural frequency, rad/sec
ω_{θ_1} = natural frequency of low-frequency complex roots of $N^\theta_{\delta_e}$ (coupled)
ω_{θ_2} = natural frequency of high-frequency complex roots of $N^\theta_{\delta_e}$ (coupled)

Subscripts

a = aileron
d = dutch roll
e = elevator
o = initial trim value
p = phugoid
r = rudder
sp = short period
SR = coupled spiral-roll subsidence (lateral phugoid)

Math Symbols

∂ = partial derivative
(a) = $(s+a)$
$[\zeta,\omega]$ = $[s^2 + 2\zeta\omega s + \omega^2]$

Presented as Paper 74-834 at the AIAA Mechanics and Control of Flight Conference, Anaheim, California, August 5-9, 1974; submitted August 21, 1974; revision received April 16, 1975. This research was accomplished for the USAF Flight Dynamics Laboratory under Contract F33615-73-C-3101.

Index categories: Aircraft Handling, Stability, and Control; Navigation, Control, and Guidance Theory.

*Principal Research Engineer. Member AIAA.
†Staff Engineer, Research. Member AIAA.

Introduction

In recent years many high-performance swept-wing aircraft have been lost in high α maneuvering due to stall-departure incidents. Departure is defined as uncommanded and/or uncontrollable motion of the aircraft[1] and may be manifest as wing rock or nose slice. Wing rock is a divergent rolling-side slipping oscillation of significant amplitude. Nose

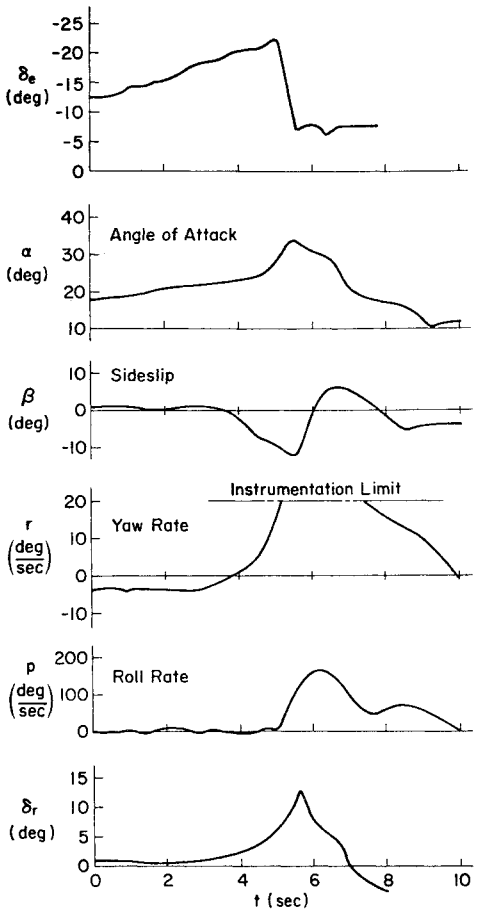

Fig. 1 A-7 stall departure (from Refs. 8 and 9).

slice is a large rapid yaw generally followed by rapid roll. Unless forward stick is applied upon first indication of departure a spin is likely to result.

Considerable research[2-7] has been conducted into possible causal factors for such departures. Analysis has generally centered around the open-loop $C_{n_{\beta_{dyn}}}$ and aileron control divergence parameters[2,6] in symmetric, uncoupled lateral-longitudinal flight. The success of these parameters in predicting departure often leaves something to be desired.

This paper presents the analytical development of, and possible physical explanation for, new open-and closed-loop parameters which arise in unsymmetric ($\beta \neq 0$) flight and appear to underlie nose slice departure of the A-7 aircraft. The initial analysis is based on a nonlinear six-degree-of-freedom digital model which incorporates aerodynamic coefficients as function of α and β. A succession of fixed-operating-point, partial-derivative expansions and linearized transfer function evaluations over a range of trim α's and β's provided the initial clues to potential key parameters. These involve the zeros of the pitch attitude numerator. Open-and closed-loop time responses from a nonlinear six-degree-of-freedom digital simulation and a simplified five-degree-of-freedom analog simulation demonstrated the phenomena. These models are validated via comparisons with actual flight traces of an A-7 departure. The closed-loop nose slice divergence phenomenon is traced through effective stability derivatives and related to previous aerodynamic flow studies. The results were further validated in a fixed-base piloted simulation.

Table 1 Significant transfer function parameter variation with change in β_0 [$\alpha_0 = 19°$]

	β_o	$1/T_S(\zeta_{SR})$	$1/T_R(\omega_{SR})$	ζ_d	ω_d	ζ_p	ω_p	ζ_{sp}	ω_{sp}
	0	.096	.425	.333	.847	.167	.165	.186	1.91
Δ	6	(.653)	(.310)	.371	.860	.139	.175	.185	2.07
	15	(−.459)	(.299)	.871	.62	.326	.199	.167	2.53

	β_o	$1/T_S(\zeta_{\theta_1})$	$1/T_R(\omega_{\theta_1})$	ζ_{θ_2}	ω_{θ_2}	$1/T_{\theta_1}$	$1/T_{\theta_2}$		
	0	.096	.425	.333	.847	−.013	.326		
$N^{\theta}_{\delta_e}$	6	(.49)	(.192)	.267	1.37	−.449	.926		
	15	(.545)	(.192)	.215	2.03	−.719	.982		

Background

The A-7 aircraft was selected for this study because very complete aero data for high α and large β were available. These data had been generated as a part of the aircraft manufacturer's investigation into its departure causes and cures. The departure of this aircraft is somewhat different from most in that it only exhibits nose slice. Figure 1 shows time traces of an actual departure.[8,9] This shows the aircraft initially in a left windup turn of about 4 deg/sec yaw rate. Sideslip is about 1 deg positive. At approximately 20 deg angle of attack ($t = 3$ sec) the yaw rate and sideslip start an aperiodic divergence. Opposing rudder is applied but cannot prevent the yaw divergence. Within two seconds the yaw rate is about 20 deg/sec positive and the sideslip 10 deg negative. At this point the rapid roll is encountered. Recovery was initiated shortly thereafter. The peak yaw rate was not recorded due to instrumentation limit but was estimated[9] at about 65 deg/sec. The ailerons were maintained at zero throughout the maneuver to prevent adverse aileron yaw from further aggravating the departure.

Stability derivatives and transfer function factors were calculated for a series of fixed operating point flight conditions approximating that for which this nose slice was recorded. However, level 1 g flight was assumed instead of a windup turn. The derivatives and transfer functions were obtained from a six-degree-of-freedom digital model employing nonlinear aerodynamic data in lookup table format. The initial analysis for symmetric flight ($\beta = 0$) showed conventional uncoupled dynamic characteristics and provided no clues to a nose slice characteristic. Since the A-7 reportedly has a pronounced tendency to change in directional trim during accelerating or decelerating flight, the effect of nonsymmetric flight was investigated. It was found that relatively small sideslip had a significant influence on the open-loop lateral-directional characteristic modes (denominator) and the pitch-attitude-to-elevator numerator zeros. All other poles and zeros were relatively unaffected.

Six-degree-of-freedom transfer function factors for three sideslip angles at $\alpha \doteq 19$ deg are shown in Table 1. The poles and zeros having the most significant change are outlined by the heavy borders. Increasing sideslip caused the roll subsidence ($1/T_R$) and spiral ($1/T_S$) to couple into a low-frequency oscillatory mode (ω_{SR}) termed lateral phugoid. The damping of this mode decreases with increasing β and it goes divergent at between 6 and 15 deg of sideslip. Comparing the dutch roll and lateral phugoid damping, it appears that there is an interchange in damping between these modes (dutch roll damping increases while lateral phugoid damping decreases). While all zeros of the pitch attitude numerator change, the most significant is the zero which appears to be the conventional speed response mode $1/T_{\theta_1}$. This root is small negative (nonminimum phase) at zero sideslip and rapidly moves to much larger negative values as sideslip increases. This nonminimum phase zero indicates a potential rapid instability upon closure of the pitch-attitude-to-elevator loop. This is of considerable concern since: 1) we would assume that pitch attitude would be tightly controlled by the pilot in high-angle-of-attack maneuvering; and 2) this would seem to indicate a longitudinal instead of lateral departure mode.

Identification of Key Parameters

Table 2 presents the nine-by-nine matrix for coupled, nonsymmetric flight obtained from the partial derivative ex-

Table 2 Matrix for coupled equations with $\beta_0 \neq 0$

$(s-X_u)$ [s + .0634]	$-X_w U_o$ [22.68]		$-X_\beta$ [5.766]			$-g\ \beta_o \cos\theta_o$ [-3.187]	$g \cos\gamma_o$ [32.024]		u	X_{δ_e} [-.1025]		X_{δ_r} [.698]	δ_e
$\frac{-Z_u}{U_o}$ [.00087]	$(s-Z_w]$ [s + .323]	-1		$\beta_o \cos\alpha_o$ [.0995]	$\beta_o \sin\alpha_o$ [.0338]				$\alpha-\alpha_o$	Z_{δ_e}/U_o [-.057]			δ_a
	$-M_\alpha$ $-M_{\dot w}Z_\alpha$ [3.577]	$s-M_q$ $-M_{\dot\alpha}$ [s + .386]	[.9 x 10^{-7}]	$r_o(\ )$ $+p_o(\ )$ [.00818]	$-r_o(\ )$ $+p_o(\ )$ [-.0025]				q	M_{δ_e} [-2.92]			δ_r
	$-Y_\alpha/U_o$ [-.0122]		$(s-Y_v)$ [s + .1062]	$-\sin\alpha_o$ [-.3216]	$\cos\alpha_o$ [.9469]	$\frac{-g}{U_o}\cos\theta_o$ [-.1166]	$\frac{-g}{U_o}\beta_o \sin\gamma_o$ [-.0129]		$\beta-\beta_o$	Y_{δ_e}/U_o [-.0037]		Y_{δ_r}/U_o [.0255]	
	$-\mathcal{L}'_\alpha$ [-3.09]		$\mathcal{L}'_\beta$ [4.45]	$(s-\mathcal{L}'_p)$ [s + .849]	$\mathcal{L}'_r$ [-.3323]				p	$\mathcal{L}'_{\delta_e}$ [-.292]	$\mathcal{L}'_{\delta_a}$ [.431]	$\mathcal{L}'_{\delta_r}$ [1.4]	
	$-N'_\alpha$ [1.486]		$-N'_\beta$ [.1885]	$-N'_p$ [-.0193]	$(s-N'_r)$ [s + .1276]				r	N'_{δ_e} [.1095]	N'_{δ_a} [.031]	N'_{δ_r} [-.998]	
				-1	$-\tan\theta_o$ [-.3396]	s	$\frac{-r_o}{\cos^2\theta_o}$ [.0116]		φ				
		-1				r_o [-.0104]	s		$\theta-\theta_o$				
					$\frac{-1}{\cos\theta_o}$ [-1.056]		$\frac{-r_o \sin\theta_o}{\cos^2\theta_o}$ [.0037]	s	$\psi-\psi_o$				

pansion of the nine equations of motion. The major derivatives are identified in literal form and, for comparison, have been evaluated at a prestall flight condition of $\alpha_0 = 19$ deg and $\beta_0 = 6$ deg. Off-diagonal terms with values two or more orders of magnitude less than the terms shown have been omitted. For the A-7, the major coupling is provided by the terms within the heavy borderlines. Two of these, L'_α and N'_α, are aerodynamic and two, $\beta_0 \cos\alpha_0$ and $\beta_0 \sin\alpha_0$, are nonlinear kinematic terms.† The "effective derivative" $Z_p \equiv \beta_0 \cos\alpha_0$ is roughly one-third the value of Z_w, while $Z_r \equiv \beta_0 \sin\alpha_0$ is about one-tenth of Z_w. Thus, one might expect these coupling terms to alter the pitch numerator zero $1/T_{\theta_2}$ since for the uncoupled case $1/T_{\theta_2} \doteq -Z_w$.[12] In the roll equation, L'_α is about three-quarters the magnitude of L'_β and of opposite sign; thus, for this trim condition (positive β), an increase in α results in a moment which tends to cancel the roll static stability. In the yaw equation, N'_α is about eight times the magnitude of N'_β and both are negative. This indicates a strong directional divergence characteristic with increasing α or β.

The influence of these off-diagonal terms on pitch attitude transfer function pole-zero locations is demonstrated in Fig. 2 Figure 2a shows a completely uncoupled six-degree-of-freedom case, for reference, in which the two lateral-directional modes (ω_{SR} and ω_d) have canceling zeros (ω_{θ_1} and ω_{θ_2}). The longitudinal poles and zeros reflect the near stall condition in which $1/T_{\theta_2}$ becomes small and $1/T_{\theta_1}$ is negative. Figure 2d presents the pole-zero location for the completely coupled six-degree-of-freedom case. Comparison of Figs. 2a and 2d shows the poles to be little affected by coupling, whereas a major shift occurs in zero location. The most significant movement is in the two real zeros because, as will be shown later, closure of the $\theta \mapsto \delta_e$ loop will drive one closed-loop root toward the right-half-plane (nonminimum phase) zero and system instability. Of secondary concern is the separation of the dutch roll dipole pair (ω_d, ω_{θ_2}) which indicates considerable modal response excitation via elevator (i.e., longitudinal to lateral coupling).

The influence of the individual pair of coupling terms is identified in Figs. 2b and 2c. In Fig. 2b the Z equation off-diagonal terms are set to zero; in Fig. 2c the L' and N' equation off-diagonal terms are removed. Individually, these coupling terms are seen to result in considerably less shift in the zeros than when all are included (Fig. 2d). A literal expansion of the numerator matrix in Ref. 13 shows the coupling derivatives to occur in multiplicative form and hence to increase the shift in zeros.

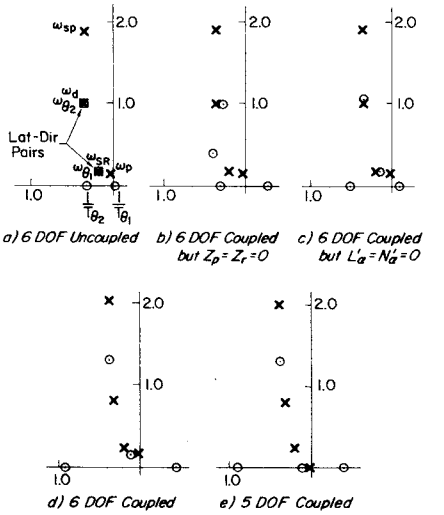

Fig. 2 Survey of $N^\theta_{\delta_e}$ approximations for $\alpha_0 = 19°$, $\beta_0 = 6°$.

†The earliest known discussion of this coupling phenomenon was documented in 1916[10] for a six-degree-of-freedom analysis of the B.E.-2 biplane in which the octals were factored by hand! This aircraft exhibited $L_\alpha \doteq L_\beta$; $N_\alpha = 2N_\beta$ and $M_\beta \doteq M_u$.

A similar development to the above but employing a five-degree-of-freedom model is presented in Ref. 11 for a swept-wing transport aircraft. The same coupling terms were found to dominate at much lower angle of attack but comparable sideslip range (e.g., 6-15 deg). In the Ref. 11 study, the coupling primarily produced an oscillatory aerodynamics/kinematic interchange in short-period energy between p and α via L_α.

As an aid in identification of the modes reflected by the poles and zeros of Fig. 2, the longitudinal dynamics were reduced to a short-period approximation by deletion of the X equation, which usually eliminates the $1/T_{\theta_1}$ zero and replaces the complex phugoid pole with a first-order pole at the origin. However, Fig. 2e shows the zeros previously identified as $1/T_{\theta_1}$ and $1/T_{\theta_2}$ to remain unchanged from the complete six-degree-of-freedom case. The complex zero previously identified as ω_{SR} has become a first-order zero near the origin. The phugoid mode is transformed into a first-order pole at the origin, as expected. Because the pole-zero configuration of Fig. 2e reflects coupled lateral-longitudinal modes (compare with Fig. 2d), the real zero in the right half plane previously labeled $1/T_{\theta_1}$ will be identified as $1/T_{\theta_3}$ in all subsequent analysis, since this is a new, coupled lateral-longitudinal mode.

Closed-Loop Control

During flight maneuvering near the stall angle of attack, use of aileron produces adverse yaw which is commonly known to contribute to departure and spin entry in most swept-wing aircraft. Pilots are constantly warned against use of aileron when at high angle of attack. Instead, maneuvers are performed with rudder or the aircraft is unloaded (i.e., α reduced) so that aileron can be safely employed. Thus, when in the vicinity of stall, longitudinal control is primary and (probably) tightly constrained to achieve the desired lift force without inducing stall. Since the pilot cannot directly see flight path or angle of attack, his primary reference is pitch attitude.

A single-loop system survey[12] for elevator control of pitch attitude with the six-degree-of-freedom coupled airframe in nonsymmetrical flight is shown in Fig. 3. The transfer function is shown in the upper left. The root locus in the top right of the figure reflects root migrations for a pure gain closure. Note that the roots starting at ω_{SR} rapidly move to the real axis and then split into two real roots; one of which moves toward $1/T_{\theta_2}$, the other moves towards $1/T_{\theta_3}$. The rapidity of the movement of these closed-loop poles towards the zeros is demonstrated by a Bode-siggy plot in the bottom half of Fig. 3. The heavy solid and dashed lines of the Bode correspond to the path of the closed-loop roots along the real (σ) axis in the root locus above. As the loop gain is increased, the complex poles emanating from ω_{SR} meet the real axis at the apex of the solid curve in the Bode-siggy plot. Further increase in gain moves one closed-loop root to a lower frequency or toward the origin while the other root moves to higher frequency and, at very high gain, asymptotically approaches $1/T_{\theta_2}$. The root that goes toward the origin passes into the right-half-plane, as shown in the root locus. This is represented in the Bode-siggy plot by the dashed line which reflects the mirror image of the closed-loop pole asymptotically approaching the $1/T_{\theta_3}$ zero at -0.3 rad. If the pilot is to achieve effective control of pitch attitude, he must close the loop so the gain line lies below the low-frequency asymptote of the Bode plot. It is obvious that this then results in a closed-loop pole in the right-half-plane. If the pilot closes the loop so that unity gain crossover is achieved in the region of 1-3 rad/sec, which covers the range of usual loose to tight piloted pitch attitude cotrol, it may be seen that the closed-loop poles will lie very close to the open-loop zeros. For example, a unity dc gain provides a crossover between 1.5 and 2.5 rad/sec and closed-loop roots at -0.28 and $+0.66$ rad/sec. The resulting first-order divergence has a time constant of about 3.6 sec.

References 8 and 9 indicate that A-7 departure recovery is best accomplished by neutralizing the cockpit controls or, preferable, "letting go" of the stick. In Fig. 3 this opens the loop and returns the aircraft roots to the stable open-loop pole position and the aircraft then should recover by itself.

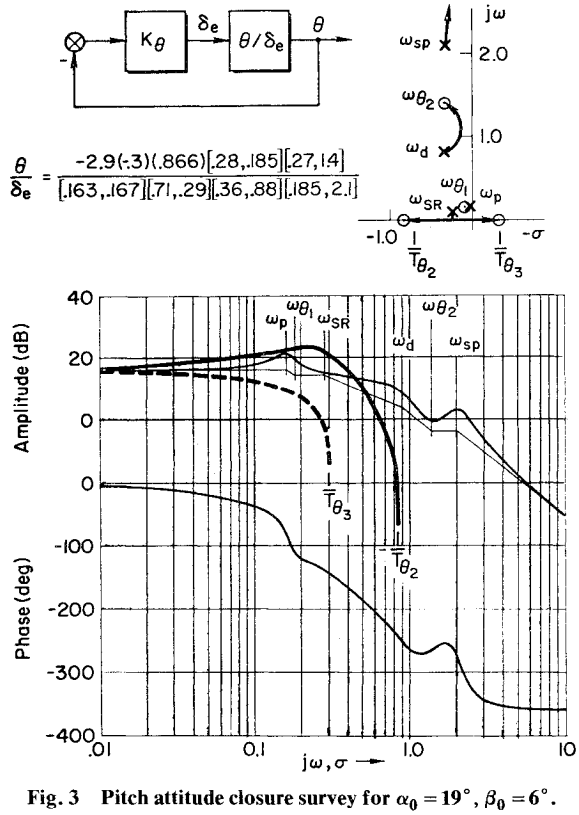

Fig. 3 Pitch attitude closure survey for $\alpha_0 = 19°$, $\beta_0 = 6°$.

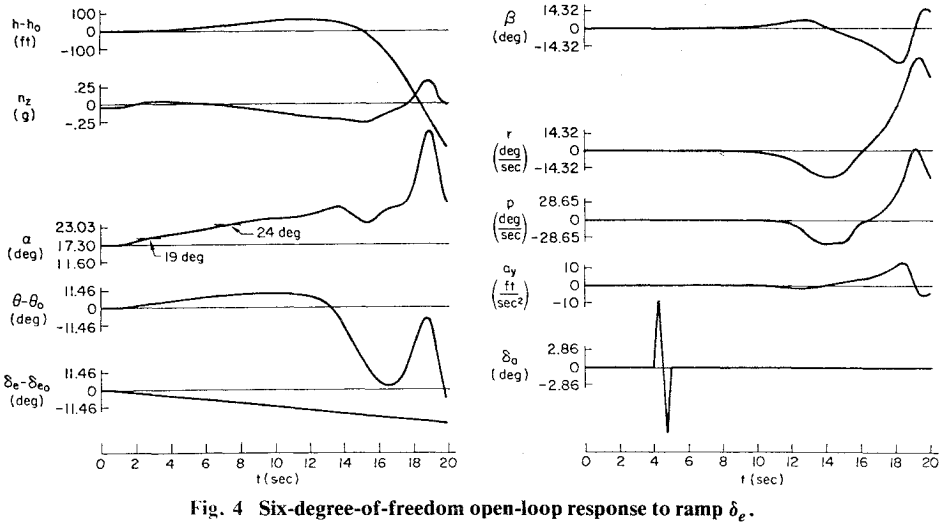

Fig. 4 Six-degree-of-freedom open-loop response to ramp δ_e.

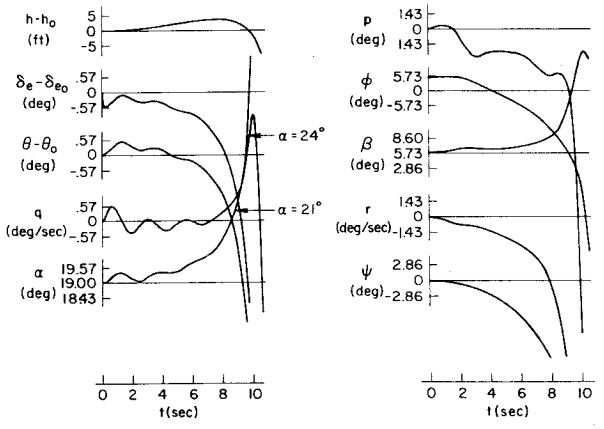

Fig. 5 Six-degree-of-freedom closed-loop response to step θ_c [$\alpha_0 = 19°, \beta_0 = 6°$].

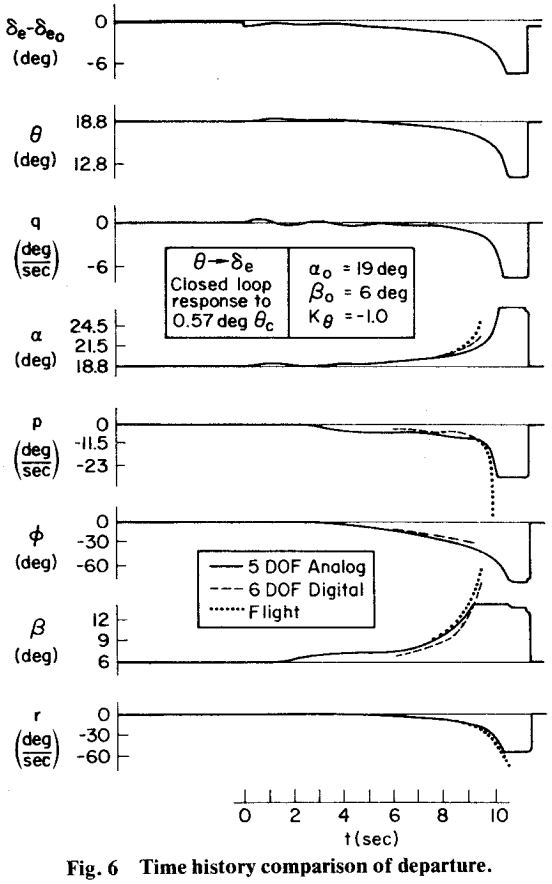

Fig. 6 Time history comparison of departure.

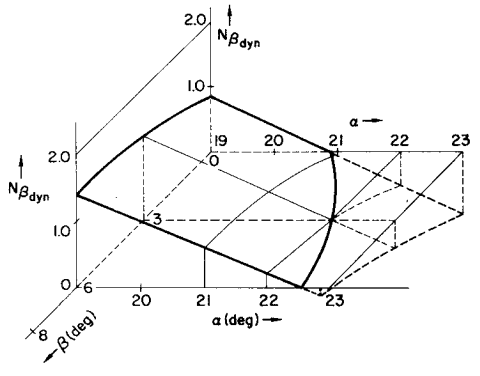

Fig. 7 Three-dimensional plot — $N_{\beta_{dyn}}$ vs α, β.

The difference in open-and closed-loop responses may be observed from time traces of a six-degree-of-freedom digital simulation using nonlinear aerodynamics. Figure 4 shows open-loop lateral and longitudinal time traces for the A-7 initially trimmed at 17.3 deg α_0 and 0 deg β_0 and with a ramp δ_e input of 1.2 deg/sec. There is no indication of instability at 19 deg α. An aileron doublet is introduced to provide some excitation of the lateral modes and it is several seconds before a slow directional divergence starts at approximately 24 deg α(9 sec). It then couples with p (and α) to form a divergent lateral oscillation with a period of approximately 11 sec. This is shown [13] to be an unstable lateral-phugoid mode. If the aircraft were trimmed at a small initial β the open-loop response would remain nearly the same but the divergence would develop at a slightly lower α because of the effect of β on the lateral phugoid damping, as noted in Table 1.

Figure 5 shows the system response when the pitch attitude loop is closed with unity gain (as in Fig. 3) and a step θ_c of

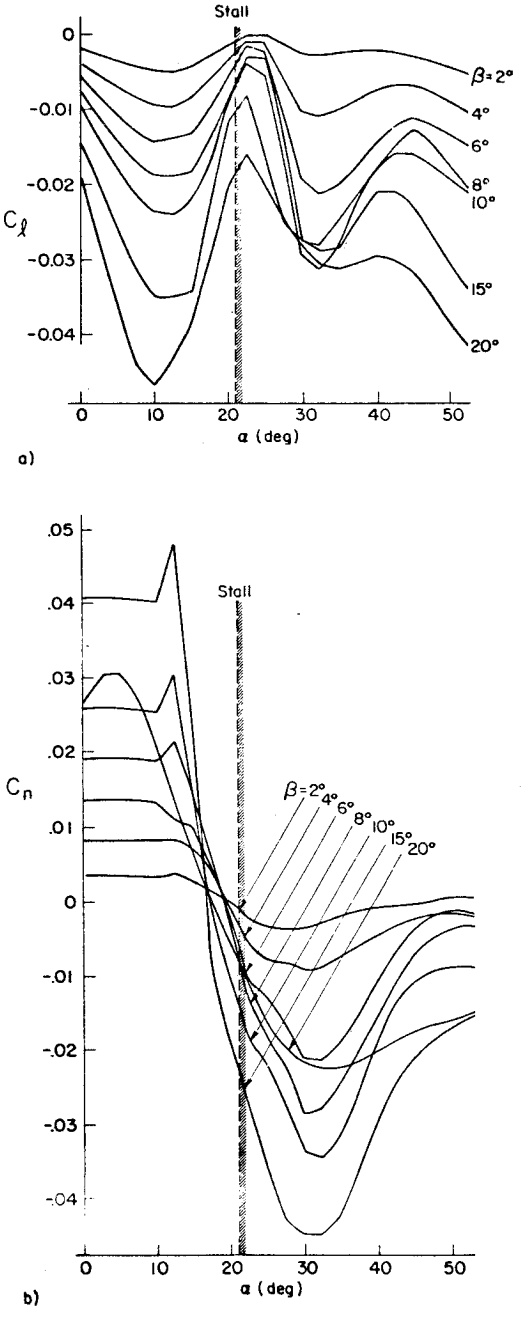

Fig. 8 $C_l[\alpha,\beta]$ and $C_n[\alpha,\beta]$; a)$C_l[\alpha,\beta,\delta_e]$ vs α at $\delta_e = -15$ deg and $0 \ll \beta \ll 20$ deg; b) C_n [α, β, δ_e] vs α at $\delta_e = -15$ deg and $0 \ll \beta \ll 20$ deg.

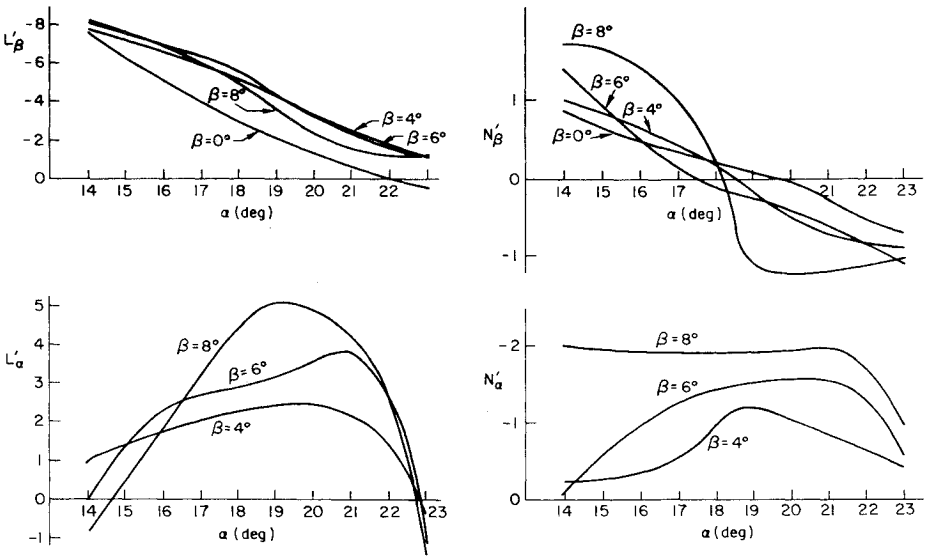

Fig. 9 Variation of L'_α, L'_β, N'_α, and N'_β with α and β.

0.57 deg is introduced. The aircraft is initially trimmed for steady flight at $\alpha = 19$ deg, $\beta = 6$ deg, and $\varphi = 5$ deg. A first-order divergence is seen to start immediately and to dominate the r, ψ, φ, θ, and α traces. The divergence time constant of 3.6 sec for the r, φ, θ, and α traces is consistent with the closed-loop right-half-plane root location predicated in Fig. 3. By the time 24 deg α is reached the aircraft is well departed. These responses verify the closed-loop mode to be coupled longitudinal-lateral motion. They also compare well with the Fig. 1 traces in that just before the high roll rate develops ($t = 9$ sec): $r \doteq -15$ deg/sec, $p \doteq -4.9$ deg/sec, and $\beta \doteq +13.5$ deg.

As a final comparison, Fig. 6 presents closed-loop time histories for the same initial conditions as in Fig. 5 but employing a nonlinear five-degree-of-freedom analog computer simulation. As in Fig. 2, the X equation has been eliminated. The dashed lines on the α, p, and β traces of Fig. 6 are the responses transcribed from the 6-DOF digital model (Fig. 5). The 6-DOF and 5-DOF traces are identical for yaw rate. The dotted curves in Fig. 6 are the responses transcribed from the actual A-7 (Fig. 1) but with the flight traces shifted in time to achieve an effective overlay of the p traces. The close agreement between the three sets of time traces is considered to be a validation of both the 5-and 6-DOF models.§

On the basis of the foregoing, it is concluded that the A-7 nose slice departure is a *closed-loop* phenomenon and the right-half-plane zero ($1/T_{\theta_3}$) of the $N^\theta_{\delta_e}$ numerator is the key parameter. The relatively close agreement between analysis, simulation traces, actual flight traces,[8] and recovery procedures recommended by LTV[9] are considered to validate our model. This conclusion is further supported by the results of the piloted simulation[13] using skilled USAF fighter test pilots.

It is interesting to compare the above result with that which would be predicted on the basis of the open-loop parameter $C_{n_{\beta\text{dyn}}}$. A three-dimensional plot of this parameter in dimensionalized form, $N_{\beta\text{dyn}}$, is shown in Fig. 7. It may be observed

§It should be noted that the yaw and roll moments causing the divergence are far greater than can be generated by full deflection of rudder and/or aileron. Analysis and simulation using pilot models[13] showed that attempts to oppose the nose slice departure with either or both of these controls results in a slight delay in departure onset; however, the surfaces rapidly reach full deflection. The surface then ceases to be of interest as a closed-loop control but becomes a static trim device. Piloted simulation[8,13] using test pilots qualified in the A-7 aircraft show that the lateral controls, if used, are driven to their stops within 1-2 sec, actually aggravate the departure, and make recovery more difficult. Thus, the results shown here for the single longitudinal loop closure are certainly valid and simplify the problem to its essentials.

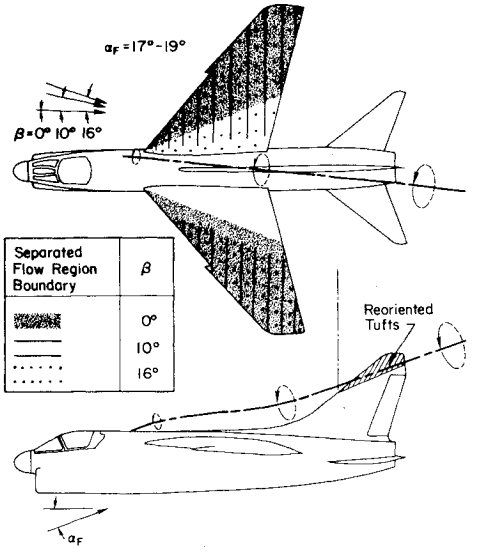

Fig. 10 A-7 wing-fuselage vortex path (from Ref. 9).

that at $\beta = 0$, $N_{\beta_{\text{dyn}}}$ becomes negative at approximately $\alpha = 21$ deg and therefore one would expect a lateral-directional divergence for higher angles of attack (e.g., Fig. 4). However, for $\beta \neq 0$ the α required for zero or negative $N_{\beta_{\text{dyn}}}$ increases. At the condition which triggered nose slice in Figs. 5 and 6 ($\alpha \doteq 19$ deg and $\beta \doteq 6$ deg) it may be seen that $N_{\beta_{\text{dyn}}} = 1.4$. Thus, this parameter is not an adequate predictor of nose slice in the A-7 aircraft. This conclusion was also reached by the aircraft manufacturer.[9]

Source of L'_α and N'_α

Preceding analysis has shown that the zero $1/T_{\theta_3}$ is strongly influenced by the stability derivatives L'_α and N'_α which, in turn, result primarily from the aerodynamic coefficients C_ℓ and C_n being nonlinear functions of both α and β. Plots of $C_\ell(\alpha,\beta)$ and $C_n(\alpha,\beta)$ are shown in Fig. 8 for positive values of β. Figure 8 indicates the slope C_{ℓ_α} is positive over the region 15-22 deg α, i.e., at positive sideslip an increase in angle of attack produces positive (right wing down) roll moment. At approximately 22-23 deg α the slope is zero, and for higher angles of attack the slope reverses. The slope also increases as trim sideslip increases. Figure 8b shows a decided break in C_{n_α} at approximately 13 deg α and large negative slope to approximately 30 deg where the slope becomes zero. For larger α this coefficient becomes positive. Thus, in the region between

13 and 24 deg α, there is a large negative (nose left) yawing moment with increase in angle of attack when at positive sideslip.

Plots of the stability derivatives L'_α, L'_β, N'_α, and N'_β evaluated specific β and α up through stall are presented in Fig. 9. Referring back to the time traces of Fig. 6, a strong correlation between the aircraft motions and the values of L'_α and N'_α can be detected. For example, Fig. 9 indicates that, at 19 deg α_0 and 6 deg β_0, L'_α and L'_β are of opposite sign and of nearly the same magnitude. Thus, with β and α increasing positively we would expect the resulting rolling moment contributions nearly to cancel. This is reflected in Fig. 6 as a relatively low roll rate up to an angle of attack of approximately 21-22 deg. Above this, L'_α changes sign, the roll moments then augment one another and, on the time traces, roll acceleration suddenly becomes very large. The derivative N'_α remains negative throughout the α range experienced in Fig. 6 and actually increases in magnitude as β increases. This results in the large negative $\dot{r}$ reflected in the time traces of Fig. 6. Thus, the departure characteristics of the A-7 appear closely related to the magnitude and sign of N'_α and L'_α up through 24 deg α (Figs. 8 or 9).

Wind-tunnel tuft studies conducted by LTV[9] provide strong evidence that the change in C_n and C_ℓ with α and β is related to two factors. One is a vortex system which originates at the intersection of the wing and fuselage (e.g., Fig. 10). The other is a separated flow which develops on the upwind wing center section, while the downwind panel flow remains attached. This induces a vortex system off the wing surface which has the same sense of rotation as the wing-fuselage vortex. The two systems reinforce each other and create a strong vortex providing a local flow redirection at the vertical tail leading edge (Fig. 10). This flow orientation would produce destabilizing forces and account for the directional stability decrease with increasing α and/or β. Thus, the combined vortex activity produces the steep slope in C_n and C_ℓ vs α, which in turn gives rise to the stability derivatives N'_α and L'_α and the nose slice parameter $1/T_{\theta_3}$.

Conclusions

The foregoing analysis and simulation have indicated that the nose slice departure of the A-7 aircraft can occur at α's considerably below the normal stall. The nose slice appears to be caused by a chain of events which evolve from directional mistrim or miscoordination of the aircraft in maneuvers. This results in sideslip and shed vortices which give rise to aerodynamic moments N'_α and L'_α. A nonlinear kinematic coupling also occurs between the sideslip and yawing or rolling of the aircraft to give rise to pseudoderivatives, Z_p and Z_r (see Table 2). These combined coupling effects result in a right-half-plane zero in the pitch-attitude-to-elevator numerator. Pilot control of pitch attitude then drives the aircraft unstable. The instability initially results in a first-order directional divergence, despite its appearance in a longitudinal numerator. The principal means of recovery is to open the pitch attitude loop, that is, to let go of the stick.

The phenomenon has been verified by open-and closed-loop time histories obtained from nonlinear six-degree-of-freedom digital and five-degree-of-freedom analog simulations. Further validation has been accomplished via a piloted simulation[13] in which nose slice characteristics were altered by varying the key coupling derivatives.

References

[1] Rutan, E.L., McElroy, C.E., and Gentry, J.R., "Stall/Near Stall Investigation of the F-4E Aircraft," FTC-TR-70-20, Aug. 1970.

[2] Weissman, R., "Development of Design Criteria for Predicting Departure Characteristics and Spin Susceptibility of Fighter-Type Aircraft," *Journal of Aircraft*, Vol. 10, April 1973, pp. 214-219.

[3] Greer, H.D., "Summary of Directional Divergence Characteristics of Several High-Performance Aircraft Configurations," NASA TN D-6993, Nov. 1972.

[4] Anglin, E.L., "Static Force Tests of a Model of a Twin-Jet Fighter Airplane for Angles of Attack from −10 Deg to 110 Deg and Sideslip Angles from −40 Deg to 40 Deg, NASA TN D-6425, Aug. 1971.

[5] Bihrle, W., Jr. and Heyman, A.C., "The Spin Behavior of Aircraft, Final Report," Vols. I-IV, GAEC Rept. 394-68-1, Dec. 1967, Grumman Aircraft Co., Bethpage, N.Y.

[6] Moul, M.T., and Paulson, J.W., "Dynamic Lateral Behavior of High-Performance Aircraft," NASA RM L58E16, Aug. 1958.

[7] Chambers, J.R. and E.L. Anglin, "Analysis of Lateral-Directional Stability Characteristics of a Twin-Jet Fighter Airplane at High Angles of Attack," NASA TN D-5361, Aug. 1969.

[8] Shields, M. E., Shaw, A.W., and Louthan, J.D., "VAC Experience in the Stall/Post-Stall and Spin Flight Regimes," *Proceedings of the Stall/Post-Stall/Spin Symposium*, Wright-Patterson AFB, Dec. 1971, pp. I-1 through I-23.

[9] Bell, M.A. and Etheridge, J.D., "A-7 Accelerated Stall Departure Study," LTV/Vought Aeronautics Div., Dallas, Texas, Rept. 2-53310/IR-5598, April, 1971.

[10] Naylor, J.L. and Jones, R., "General Mathematical Investigation of the Stability of the Motion of an Aeroplane, (V) Numerical Illustrations in the Case of Side-slipping without Turning," NACA R&M 258, Sept. 1916,

[11] Porter, R.F. and Loomis, J.P., "Examination of an Aerodynamic Coupling Phenomenon," *Journal of Aircraft*, Vol. 2, Nov.-Dec. 1965, pp. 553-556.

[12] McRuer, D.T., Ashkenas, I.L., and Graham, D., *Aircraft Dynamics and Automatic Control*, Princeton University Press, Princeton, N.J., 1974.

[13] Johnston, D.E., Ashkenas, I.L., and Hogge, J.R., "Investigation of Flying Qualities of Military Aircraft at High Angles of Attack," AFFDL-TR-74-61, May 1974; Air Force Flight Dynamics Lab., Wright-Patterson Air Force Base, Ohio.